Vertical Structure and Seasonal Variability of the Inflow to the Lofoten Basin Inferred From High-Resolution Lagrangian Simulations

Johannes S. Dugstad[1] , **Inga Monika Koszalka[2,3]**, **Pål Erik Isachsen[4,5]** , **Knut-Frode Dagestad[6]** , and **Ilker Fer[1]**

[1]Geophysical Institute, University of Bergen and Bjerknes Centre for Climate Research, Bergen, Norway, [2]Department of Meteorology, Stockholm University and the Stockholm University Baltic Sea Centre, Stockholm, Sweden, [3]Bolin Centre for Climate Research, Stockholm, Sweden, [4]Department of Geosciences, University of Oslo, Oslo, Norway, [5]Norwegian Meteorological Institute, Oslo, Norway, [6]Norwegian Meteorological Institute, Bergen, Norway

Abstract The Lofoten Basin in the eastern Nordic Seas plays a central role in modifying the warm Atlantic Water inflow toward the Arctic Ocean. Here, the Atlantic Water experiences increased residence times, cooling, and substantial transformation. In this study, we investigate the Atlantic Water inflow pathways to the Lofoten Basin and their vertical and seasonal variations using 2-D and 3-D Lagrangian simulations forced by a high-resolution ocean model. Atlantic Water enters the basin from all directions, but we find two main inflow pathways at all vertical levels, one close to the Lofoten Escarpment in the southeast, associated with the Slope Current, and another close to the Helgeland Ridge in the southwest, associated with the Front Current. The surface inflow exhibits a stronger seasonal forcing than the inflow at depth as well as a stronger heat loss that is dominated by water masses entering the basin from the south. At deeper levels, the warm inflow from the east cools, while the relatively colder inflow from the west warms. The 2-D and 3-D synthetic trajectories show similar pathways. However, they are affected differently by the seasonal signal, giving different heat exchange patterns. Our results have implications for how results from Lagrangian observations in the region should be interpreted.

Plain Language Summary The Lofoten Basin in the Nordic Seas is of fundamental importance for the modification of the warm northward flowing Atlantic Water. Much of the ocean heat is lost to the atmosphere in this region. This is maintained by warm water inflows from regions around. Here, we study these inflows, their vertical structure, seasonal variability, and contribution to the heat budget in the basin. We apply an ocean model to advect purposefully released particles in the Nordic Seas seeded at 15-, 200-, and 500-m depth and study their pathways and fates. We analyze both a horizontal 2-D (particles are fixed at depth) and a full 3-D (particles can move in the vertical) simulation and compare the two. We find that the water masses mainly enter the Lofoten Basin in two regions, one in the southeast and one in the southwest. However, the vertical structure reveals that water that is cooled enter the basin via different routes at the surface than at deeper levels. The seasonal variations are also larger at surface than at depth. The 2-D and 3-D simulations show overall similar patterns, but the 3-D simulation reveals larger seasonal variations than the 2-D simulation.

1. Introduction

The Lofoten Basin (LB) in the Norwegian Sea is recognized as a region for the retention and modification of the warm and saline Atlantic Water (AW) carried by the Norwegian Atlantic Current (NwAC) northward toward the Arctic Ocean (Koszalka et al., 2011; Mauritzen, 1996; Rossby et al., 2009). As the AW enters the Nordic Seas (a joint name for the Greenland, Iceland, and Norwegian Seas), the NwAC splits into two branches, the Slope Current and the Front Current embracing the LB to the east along the upper Norwegian continental slope and to the west along the Helgeland-Mohn Ridges, respectively (Orvik & Niiler, 2002; see also Figure 1a). The relatively warm AW spreads between the branches and experiences increased residence times in the basin (Rossby et al., 2009). Large surface heat and buoyancy loss in winter result in cooling (Isachsen, 2015; Rossby et al., 2009; Richards & Straneo, 2015), and the modified water masses sink and form a warm anomaly at depth, compensated by their high salinity (Bosse et al., 2018; Segtnan et al., 2011). The
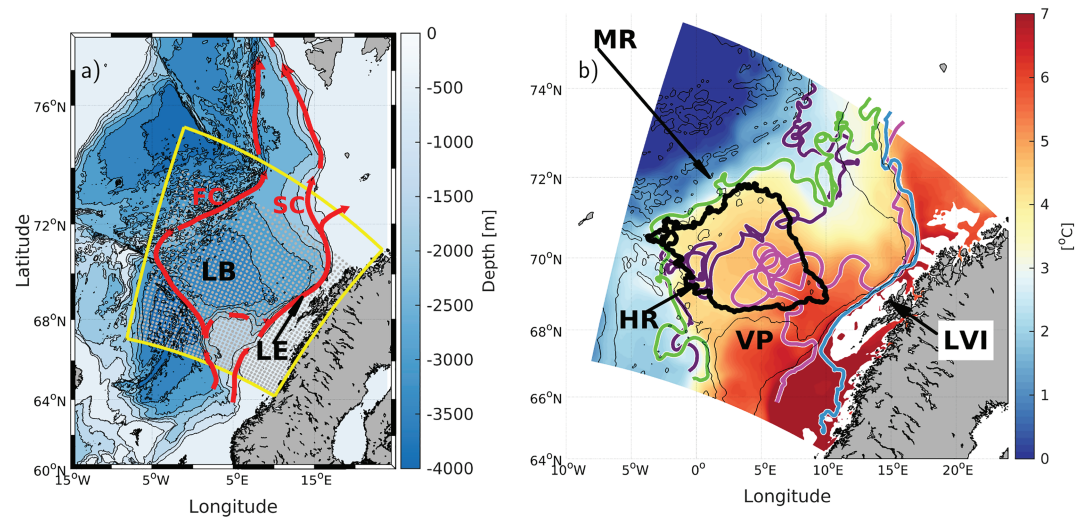
Figure 1. (a): Bathymetry map of the Nordic Seas showing the main pathways of the northward flowing Atlantic Water (red, the Slope Current, SC, and the Front Current, FC), the study domain (yellow) of the ROMS model used for the OpenDrift simulations, and the deployment grid for the synthetic drifters (gray dots). (b) ROMS model Eulerian temperature field at 200-m depth averaged over a period of 1996–1999. Superimposed are selected trajectories of 3-D synthetic drifters deployed at 200 m, illustrating pathways of the SC, (blue trajectory), FC (green trajectory), and the inflow to the LB via the Lofoten Slope Inflow (magenta) and the Helgeland Inflow (purple). Abbreviations are: LB = Lofoten Basin, LE = Lofoten Escarpment, HR = Helgeland Ridge, MR = Mohn Ridge, VP = Vøring Plateau, LVI = Lofoten-Vesterålen Islands, FC = Front Current, and SC = Slope Current.

AW extends vertically to a mean depth of 500–600 m and a maximum depth of approximately 800 m (Bosse et al., 2018; Mauritzen, 1996) (see also Figure 1b). Quantifying and understanding processes that modify the AW en route to the Arctic are important with implications for the regional climate and marine ecosystems (Årthun et al., 2018; Kovacs et al., 2011; Ogawa et al., 2018), as well as impacts on the Arctic sea ice cover (Årthun et al., 2019).

Quantifying the spatial distribution and temporal variability of mass and heat exchanges between the AW inflow and the LB is not a trivial task, as complex transient and mesoscale (10–100 km) processes contribute with large eddy heat fluxes (Isachsen et al., 2012; Spall, 2010). Several studies have pointed to the role of mesoscale eddies shed from the Slope Current off the Lofoten Escarpment and advected westward to the LB (Isachsen et al., 2012; Isachsen, 2015; Köhl, 2007; Raj et al., 2016; Volkov et al., 2015). This view is consistent with enhanced eddy kinetic energy densities and horizontal diffusivities in the eastern part of the LB as inferred from surface drifter data (Andersson et al., 2011; Koszalka et al., 2011). Subsurface acoustic RAFOS float trajectories have also shown eddy variability in this region (Rossby et al., 2009).

Analyses of hydrographic observations (Ivanov & Korablev, 1995) and model studies (Köhl, 2007; Volkov et al., 2013) have suggested that anticyclonic eddies from the Slope Current follow a cyclonic path toward the center of the LB. Volkov et al. (2013) also suggested that this cyclonic pattern is more pronounced in deeper levels (1,000–1,500 m). Furthermore, using subsurface RAFOS float observations, Rossby et al. (2009) showed that the flow at 200-m depth is strongly topographically steered. A large fraction of the RAFOS floats followed the Slope Current and entered the LB from east, trapped in eddies shed from the slope. However, analyses of surface drifters by Koszalka et al. (2013) and Dugstad et al. (2019) have suggested that the warm AW spreads and enters the LB from the south as a broad slab between the two NwAC branches, thus indicating a different pattern at the surface. In particular, the latter study found that the surface drifters with long residence time inside the basin enter along the southern part of the LB , mainly across the northern rim of the Vøring Plateau. In an attempt to partition the contribution of advective heat transport into the LB in their eddy-permitting model, Dugstad et al. (2019) found that the heat transport by the mean flow was important in upper layers along the southern sector of the basin, while the eddy heat fluxes from the Lofoten Escarpment in the east were enhanced at depths between 300 and 600 m. While the above studies suggest that both the mean flow and eddy fluxes contribute to the heat budget of the LB, the main routes

and vertical structure of the AW inflow to the basin, the associated heat exchange, and the temporal aspect of these exchanges remain poorly known.

We address these questions by analyzing trajectories from Lagrangian simulations driven by outputs from a 800-m horizontal resolution ocean model of the region. We investigate the main inflow routes, describe their vertical structure and seasonal variability, and estimate how this affects the AW-LB heat exchange. We analyze two Lagrangian simulations, one with only 2-D horizontal advection (similar to the motion of surface drifters and RAFOS floats) and one that also allows vertical advection (3-D), and compare the two. Deployments at three vertical levels (15, 200, and 500 m) are used to quantify the vertical structure of the AW-LB exchange. Our study thus complements Dugstad et al. (2019) who addressed the subsurface AW-LB exchange within the Eulerian framework only. Using the Lagrangian framework, we are able to study the pathways and fates of a particular water mass, namely, AW, as it enters and passes through the LB.

2. Data and Methods

2.1. Ocean Model

We integrate Lagrangian trajectories using the output from a high-resolution Regional Ocean Modeling System (ROMS) configuration for the eastern Nordic Seas. ROMS is a hydrostatic primitive equation model defined on a staggered C-grid and terrain-following vertical coordinates (Haidvogel et al., 2008; Shchepetkin & McWilliams, 2005, 2009). A fourth-order-centered scheme is used for vertical advection and a third-order upwind scheme for horizontal tracer and momentum advection. No explicit horizontal eddy viscosity or diffusion is applied but the upwind advection scheme exhibits implicit numerical diffusion. Unresolved vertical mixing processes are parameterized using the k-ϵ version of the General Length Scale scheme (Umlauf & Burchard, 2003; Warner et al., 2005). The skill of this scheme in representing vertical convection is satisfactory (Warner et al., 2005), and its effect on our results and interpretation is discussed in section 4.3. The open lateral boundaries are relaxed toward monthly fields from the Global Forecast Ocean Assimilation Model (MacLachlan et al., 2015), and the atmospheric forcing is provided by 6-hourly fields from the ERA-Interim atmospheric reanalysis (Dee et al., 2011). The model has 800-m horizontal resolution and 60 vertical layers with enhanced resolution near the surface (thickness varying from 2 to 5 m at surface toward 60 to 70 m toward the bottom). Model output (currents and hydrography) is stored every 6 hr for the period of 1996–1999. With this spatial and temporal resolution the model resolves mesoscale and even some submesocale processes (Isachsen, 2015; Trodahl & Isachsen, 2018) and thus captures the circulation features that dominate lateral stirring processes.

2.2. Lagrangian Simulations

For Lagrangian simulations, we employ OpenDrift (Dagestad et al., 2018), an open source Python-based framework for Lagrangian modeling, which operates off-line, that is, using a stored model velocity output. OpenDrift includes modules to simulate drift of various substances and objects such as oil, search and rescue, and plankton (Dagestad & Röhrs, 2019; Jones et al., 2016; Kvile et al., 2018). In this study, however, we follow the movement of water particles, using the most basic OpenDrift module for passive tracers advected solely with ocean currents. We will refer to the Lagrangian simulations as "synthetic drifters" to distinguish them from real surface drifter observations used for comparison (section 2.3). Two experiments of synthetic drifters are performed, using either only the horizontal velocity (2-D experiments) or the full three-dimensional velocity field (3-D experiments). Lagrangian positions are updated using the 6-hourly model currents by applying a fourth-order Runge-Kutta integration routine. Trajectories, that is, time series of Lagrangian positions (longitude, latitude, and depth) are stored with 6-hr intervals. ROMS potential temperature, salinity, and velocity outputs are linearly interpolated on the particle trajectories. We do not apply explicit lateral or vertical diffusion to avoid making trajectories too diffusive with respect to transport properties of the ROMS model solution used to force them. The question of adding additional diffusive term to compensate for the missed variability in off-line Lagrangian simulation has been a subject of a discussion but is usually avoided in studies using high-resolution model outputted at high frequency; see for example, Bower et al. (2011), Gelderloos et al. (2017), Rühs et al. (2019), and in our previous study, Dugstad et al. (2019), as well as van Sebille et al. (2018) and Wagner et al. (2019) and references herein. We will come back to this point in section 4.

The synthetic drifters are deployed at three levels, 15, 200, and 500 m (typical anchoring levels for surface drifters and RAFOS floats, respectively, and reaching down to the base of the AW in the Nordic Seas), and uniformly over the horizontal domain (marked in Figure 1a) in sets of 40 × 40 drifters (about 20-km spacing

Table 1
Statistics for the Entry Into the LB and Residence Time for Synthetic Drifters (2-D and 3-D Lagrangian Experiments)

			Lofoten Basin Drifters		Residence time [days]	
	Depth [m]	Total	all	outside [%]	all entries (LSI) (HI)	longest stay (LSI) (HI)
2D						
	15	164,013	99,588	60,432 [48]	10 (8) (13)	29 (19) (37)
	200	171,566	100,977	61,841 [47]	12 (10) (14)	39 (28) (44)
	500	143,455	92,759	53,603 [51]	16 (14) (19)	56 (47) (62)
3D						
	15	163,456	100,886	61,730 [49]	11 (10) (14)	35 (25) (43)
	200	164,227	102,304	63,148 [50]	13 (11) (15)	42 (32) (48)
	500	143,891	92,209	53,053 [51]	17 (14) (22)	59 (43) (76)

Note. Total: the total number of synthetic drifters considered in the analysis (see section 2.2). Lofoten Basin Drifters: the number of synthetic drifters interacting with the LB, both given by *all* drifters (both those deployed in the LB and those entering from outside) and the ones only entering the basin from *outside* (all minus the 39,156 drifters deployed in the LB). The percentage of drifters entering from outside, calculated as $\frac{outside}{Total - 39,156} * 100$, is given in brackets. Residence time, all entries: the mean residence time for all synthetic drifter entries in the LB. Residence time, longest stay: the mean residence time for the longest stay in the basin (see section 3.2). The residence times in parentheses are given for drifters entering the basin across the LSI and HI segments, respectively.

between the deployments). The sets of 1,600 drifters are deployed every week from 1 January 1996 to 1 January 1999, giving 156 weeks of deployments ($1,600 * 156 = 249,600$ drifters in total at each seeding depth). Each synthetic drifter is given a lifetime of 1 year. We disregard the deployments over shelf areas shallower than 200 m, which reduces the number of trajectories to 225,000 at 15 and 200 m and 195,000 at 500 m, and we apply absorbing boundary conditions that cause drifters that run over a shelf region shallower than 200 m or hit the open-ocean boundary of the model to be terminated. We also exclude from the analysis drifters that are deployed north of the northernmost part of the LB contour (26,988 drifters for each level, 2-D and 3-D), and about 15% of the total that are deployed in a cyclonic rim circulation of the Norwegian Sea to the south and recirculating southward and never reaching the LB.

The total number of analyzed synthetic drifters, for each vertical level and experiment, is given in Table 1. Furthermore, since we focus on the inflow to the LB, we will in most cases consider only the drifters entering the LB from outside (Table 1). As in Dugstad et al. (2019), we define the LB by the 3,000-m isobath (see highlighted black contour in Figure 1a). This contour is closed except in the southwest corner where the Helgeland Ridge opens toward the Norwegian Basin. We manually closed this 28-km-long segment.

2.3. Relative Dispersion of Real and Synthetic Drifters

To evaluate the velocity field in the model, we compare the Lagrangian trajectories deployed at 15-m depth to actual surface drifter observations using dispersion statistics. Surface drifter data from the eastern Nordic Seas (15–20° E, 62–75° N) were downloaded from the Global Drifter Programme database (https://www.aoml.noaa.gov/phod/gdp/ updated through 30 June 2018 at the time of download on 19 January 2019). The drifter positions (longitude, latitude) were quality controlled and interpolated via a kriging method to 6-hr intervals by the AOML/NOAA Drifter Data Assembly Center (Lumpkin & Pazos, 2007). This type of drifter consists of a surface buoy, with a transmitter and a temperature sensor and a subsurface drogue at 15-m depth. The drifter has a tether strain sensor for monitoring the presence of the drogue. Only trajectory segments with the drogue attached were used. The largest contribution to the total of 370 drifters came from the POLEWARD experiment under the International Polar Year (2007–2009) whereby 150 drifters were deployed at the Svinøy site (63° N), near the islands of Gimsøy, Bjørnøya, in the Barents Sea, and in the LB (Koszalka et al., 2009). Most of the POLEWARD drifters were deployed in pairs and triplets yielding nearly 100 drifter pairs. A smaller deployment (10 drifters) was also carried out during the ProVoLo experiment.

We evaluate the Lagrangian simulations by comparing the 2-D synthetic drifters deployed at 15-m depth with the observed surface drifters anchored at 15-m depth, using a relative dispersion statistics. The relative dispersion quantifies the spreading of nearby drifters due to spatial differences in the velocity field and can be regarded as a proxy for Eulerian wave number kinetic energy spectra (Koszalka et al., 2009; LaCasce, 2008). As in Koszalka et al. (2009) we consider chance pairs (drifters that came close together at any instant
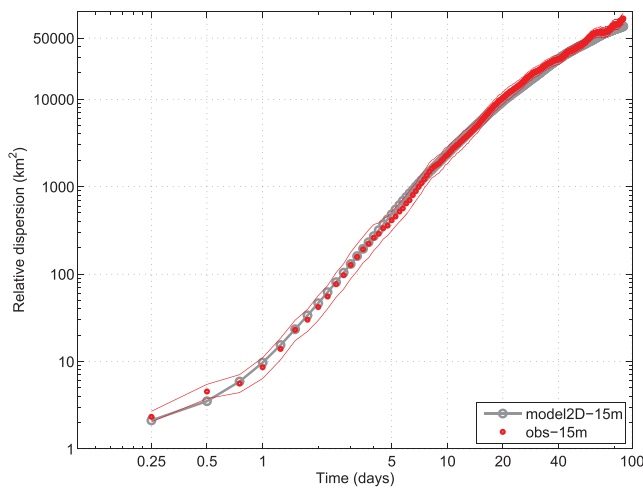
Figure 2. Ensemble-mean relative dispersion as a function of time for the observed surface drifters and for the 2-D synthetic drifters deployed and advected at anchoring depth of the surface drifters (15 m). The 95% confidence intervals for the observed relative dispersion are shown with red thin lines.

of time, not necessarily deployed together) and close separations (less than 2 km) . In addition, to avoid the drifter pair velocities that are correlated at the starting point of the analysis, we search pairs at 1-day intervals. This yields 461 chance pairs for the observed surface drifters (reduced by half after 100 days). For the synthetic trajectories, due to their larger number, we find pairs at 30-day intervals yielding over 200,000 pairs for the total duration of the experiment. This large number of drifters allows a statistical comparison.

The ensemble-mean relative dispersion of the synthetic and observed drifters is shown in Figure 2. The synthetic drifters reproduce the relative dispersion of the surface drifters very well. Both the initial exponential regime during the first 2 days and the Richardson regime at 2–10 days (Koszalka et al., 2009) are captured. This means that the near-surface turbulent transport processes including stirring by eddies and mean current shear are statistically well represented by the ROMS model output forcing the Lagrangian simulations. Unfortunately, a small number of the available RAFOS floats (∼20) in the eastern Nordic Seas prohibits a similar statistical evaluation at deeper levels.

3. Results

3.1. General Circulation Features

We first focus on the general circulation at 200 m, which is representative for the AW inflow in the eastern Nordic Seas, as the flows in this region are relatively weakly stratified and to a large extent steered by topography.

Figure 1a shows a schematic of mean currents superimposed on a bathymetric map, and Figure 1b shows the model domain and the model's time-averaged temperature field at 200 m carrying a signature of the warm AW filling the LB. Superimposed are four selected synthetic Lagrangian trajectories from the 3-D deployment at 200-m depth that illustrate main circulation features discussed in the text: the northward flowing Slope Current (blue) and Front Current (green) and two main inflow pathways to the LB from the east and west, given in magenta and purple colors, respectively (the inflows will be further discussed below). Similar circulation patterns are also identified in the 2-D synthetic drifters deployed at 200 m (not shown), and they are also evident in trajectories of the observed RAFOS floats ballasted at ∼250-m depth (Rossby et al., 2009).

3.2. Main Inflow Pathways and Residence Times in the LB

In order to visualize the main inflows to the LB, we plot "drifter density maps." These are obtained by counting occurrences of individual synthetic drifters in a grid of longitude-latitude bins and normalizing by the total number of drifters entering the LB. Figure 3 shows such maps to indicate pathways of drifters before LB entry, using drifters deployed at 15 and 500 m. Since a drifter can cross the LB contour several times, we consider trajectory segments from deployment until the entry of the longest period of stay in the basin. (When a drifter crosses the basin contour multiple times, it experiences several periods in the basin. One of the periods must be longer than the other ones. We refer to this as the longest period of stay, or simply the "longest stay.") Because the LB is located at high latitudes (around 70° N), the longitude bins are scaled by a factor $1/\cos(70°)$ relative to the latitude bins. Thus, we choose bin sizes of 0.73° × 0.25°. Only density maps from the 3-D simulation are shown in Figure 3, but the ones derived from 2-D simulations are similar. There are drifters entering the LB from all sides, but two major inflow regions stand out: the "Lofoten Slope Inflow" (LSI) to the southeast, close to the continental slope, and the "Helgeland Inflow" (HI) to the southwest, approximately where the 3,000-m contour does not close. These two inflow regions are marked with cyan segments in the figure. The importance of the LSI and HI is quantified by counting the number of drifters that entered the basin (for their longest stay) across these segments. The segment lengths amount to 16% (LSI) and 18% (HI) of the total LB contour length, but the percentage of drifters with a longest stay entry across these segments is larger. In the 3-D simulations LSI accounts for 24–25% of the drifters at all three levels, whereas for the HI the percentage of drifters increases from 17% at 15 m to 25% at 500 m. Results from the 2-D simulations agree to within 2%. This means that approximately 50% of the drifters
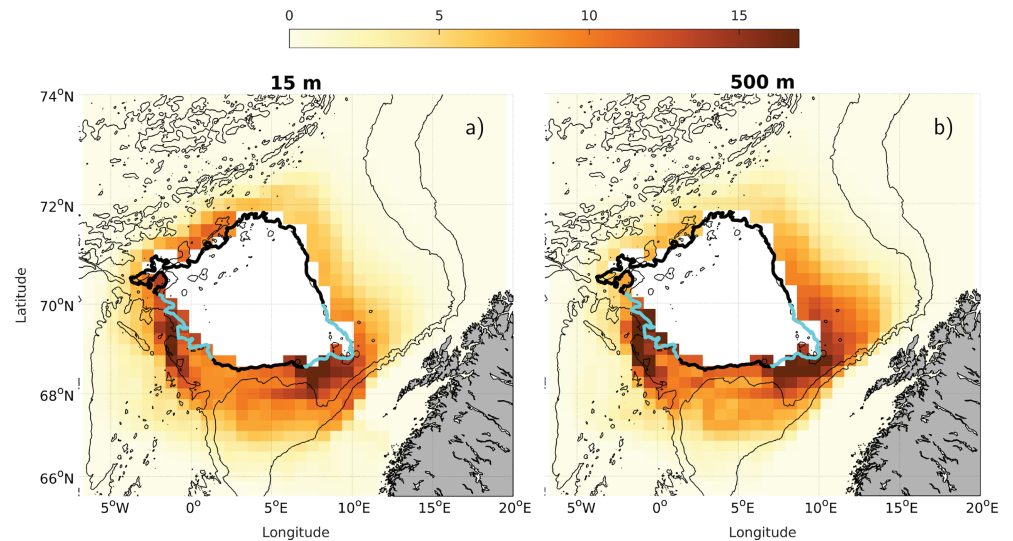
Figure 3. Density maps of 3-D synthetic drifters deployed at (a) 15 m and (b) 500-m depth entering the LB for their longest stay in the basin. Only segments from deployment until the longest stay entry are considered. The 1,000- and 2000-m isobaths are shown in black thin lines, and the 3,000-m isobath (thick black) defines the LB. The density maps show the occurrence percentage of drifters in a grid of longitude-latitude, relative to the number of drifters entering the basin for the respective deployment depth. The bin sizes are 0.73° × 0.25° (see section 3.2). Cyan segments show the LSI and HI segments along the LB contour.

enter the basin via the LSI and the HI segments combined, which is disproportionally large compared with the relative length of the segments. Hence, these inflows appear as key regions for the AW-LB exchange.

In general, the salient circulation features in the region are related to topography and thus appear similar in the 2-D and 3-D synthetic trajectories (Table 1). In both, the 2-D and 3-D simulations, similar percentages of synthetic drifters interact with the LB (~50%). The simulations also agree well in terms of residence times inside the LB. We report averages over two alternative residence times computed from the trajectories, the residence time of any entry to the basin (this can include short duration crossings of the basin contour) and the residence time of the longest stay. In both 2-D and 3-D simulations, the mean residence time for all entries is shortest for drifters deployed at 15 m (10 days) and longest for drifters deployed at 500 m (17 days). The same holds for the longest stay entries (30 and 60 days for drifters deployed at 15 and 500 m, respectively) indicating that the residence times increase with depth. If only sampling for the trajectories entering the LB across the LSI or HI segments (cyan segments in Figures 3a and 3b), the residence times also agree fairly well. The largest difference is seen for drifters deployed at 500-m depth and entering the LB via HI, where the longest stay residence time for the 3-D simulation is larger (76 vs. 62 days). The residence times are generally longer for the HI entries compared to the LSI entries (discussed in section 4.1).

Note that the synthetic drifters are integrated for only 1 year so the residence time statistics are likely underestimated with respect to an asymptotic case of infinite time or a multiyear integration; nevertheless, it is a useful diagnostic for the purpose of questions addressed in our work. The differences between the 2-D and 3-D simulations, their seasonal variation, and impact on heat exchange are further considered in sections 3.4–3.5.

3.3. Vertical Structure of the Inflow and Its Seasonal Variations in 3-D Lagrangian Simulations

Probability density functions (PDFs) of the depth of entry to the LB are calculated for the first entry and the longest stay entry using the 3-D synthetic drifters (Figure 4a). The PDF curves show that the majority of drifters enter the basin close to their deployment level, but they are skewed toward deeper levels, implying that more drifters have sunk relative to their deployment position.

To study the differences in vertical drifter movements, we calculate a monthly breakdown of the relative vertical displacement between the deployment position and the entry to the LB. Specifically, for each 3-D synthetic drifter with a longest stay entry in a given month, we compute its vertical displacement relative to its depth 30 days prior to entry (i.e., difference in depth at time of entry and 30 days earlier). The choice of a 30-day window was made to ensure a time span long enough to allow the drifters to be affected by
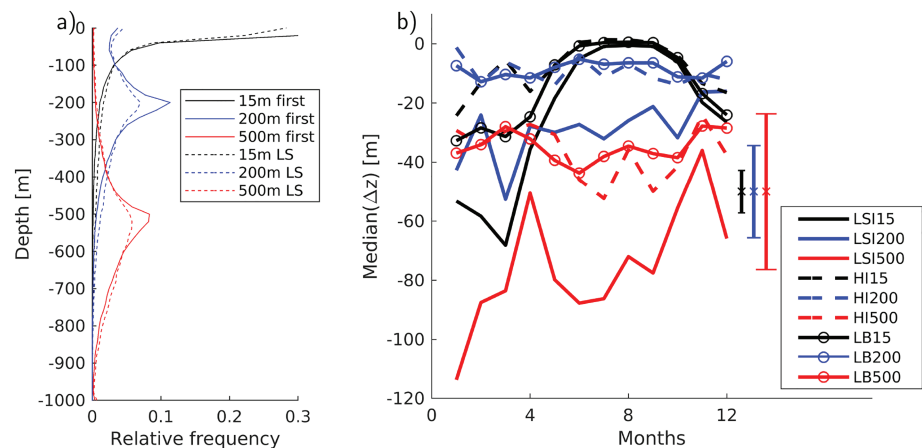
Figure 4. (a): Probability density functions (PDFs) of the entry depth into the LB for 3-D drifters for the first entry to the basin (solid) and the longest stay (LS, dashed); (b) seasonal median vertical displacements (negative = sinking) experienced by synthetic drifters between the day of their longest stay entry and 30 days earlier; for example, Month = 1 shows the median vertical displacement between the longest stay entry and 30 days before for drifters entering the basin in January. We show vertical displacements for drifters entering via the LSI (solid lines), HI (dashed lines), and the entire LB (solid lines with circles). Error bars for LSI15, LSI200, and LSI500 are also shown (see text). Error bars for other groups are similar. The LSI and HI are defined as the cyan-colored segments in Figures 3a and 3b.

different physical processes but also short enough as the time span should be shorter than the seasonal variability. A representative vertical displacement for the given month is obtained as the median value of all vertical displacements in that month (a negative vertical displacement indicates sinking). The ROMS vertical resolution gets coarser at depth. This imposes an inherent uncertainty in the vertical displacement in the Lagrangian simulations. We quantify this uncertainty using the model layer thickness (annual average) at the depth of the estimated median vertical displacement. The error bars increase with depth and are only shown for LSI for clarity (the geographical difference is not large).

The month-to-month calculations are done separately for the entries across the LSI and HI segments as well as for the entire basin contour as a comparison (Figure 4b). The drifter densities 30 days prior to the entries across LSI and HI, respectively, indicate that the drifters are concentrated around their respective entry regions (not shown). Thus, the drifters have not traveled from vastly different regions during this period; hence, they have not experienced particularly different physical processes, suggesting that our 30-day window is an appropriate choice. For all three categories, a seasonal signal is seen in surface layers (drifters deployed at 15 m) where winter months are characterized by a net sinking while summer months show drifter movements with negligible vertical displacement. Deep mixed layers in winter allow larger vertical displacements than a stratified water column in summer. The seasonal signal is also stronger for drifters entering via the LSI than via the HI or the basin as a whole, and the variations are strongest at the surface. At deeper levels (especially 500 m), the error bars are large, and the difference in vertical displacements is not statistically significant. But in general, Figure 4b implies a different vertical structure of the inflows in winter than in summer and that the net sinking is largest in the LSI region, indicating that waters entering here are the most buoyant and therefore most susceptible to cooling (with consequent sinking) in winter.

As the 3-D synthetic drifters are advected vertically, they enter the LB at various depths. Taking advantage of the spatially uniform deployment over the area, we further categorize the drifters based on the depth of the longest stay entry to the LB, independent of their initial deployment level. From the PDFs in Figure 4a, we find "break points" in drifter densities (where the various PDFs intersect) and use them to define three entry depth classes: (1) 0–130 m (62,355 drifters), (2) 130–370 m (51,915 drifters) and (3) 370 m to bottom (63,661 drifters). From this definition, a drifter that, for example, had its longest stay entry to the LB at 40-m depth would be defined to belong to Depth Class 1. The 3-D synthetic drifters in these three classes are further subdivided by which season they enter the LB (winter: January–March and summer: July–September).

As discussed above, the drifters experience sinking during winter, while during summer, the strong stratification restricts the drifters to float near their deployment level. This seasonal difference manifests itself as a smaller percentage of drifters being observed in Depth Class 1 during winter compared to summer, and
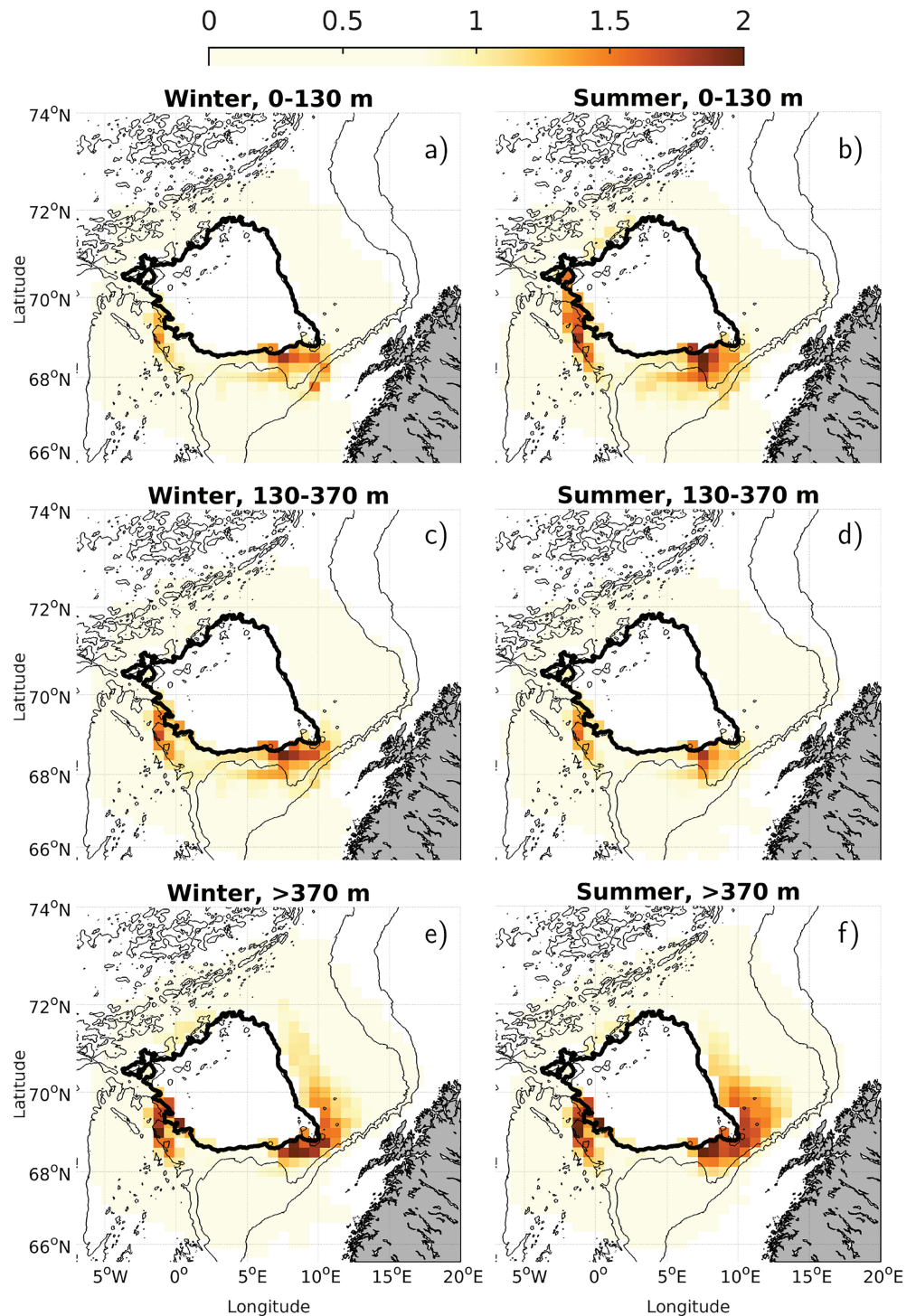
Figure 5. Density maps of 3-D synthetic drifters entering the LB in different seasons: (a, c, and e) Winter = January–March and (b, d, and f) Summer = July–September, and at different depths. Only trajectory segments from deployment until the longest stay entry are considered. The entry depth classes (see text) are 1:0–130 m (a,b), 2:130–370 m (c,d), 3:370–bottom (e,f). The color bar shows the percentage of drifters in a bin when normalized with the total number of drifters entering the basin summed over all depth classes (62,355 + 51,915 + 63,661 = 177,931). Bin sizes are as in Figure 3.
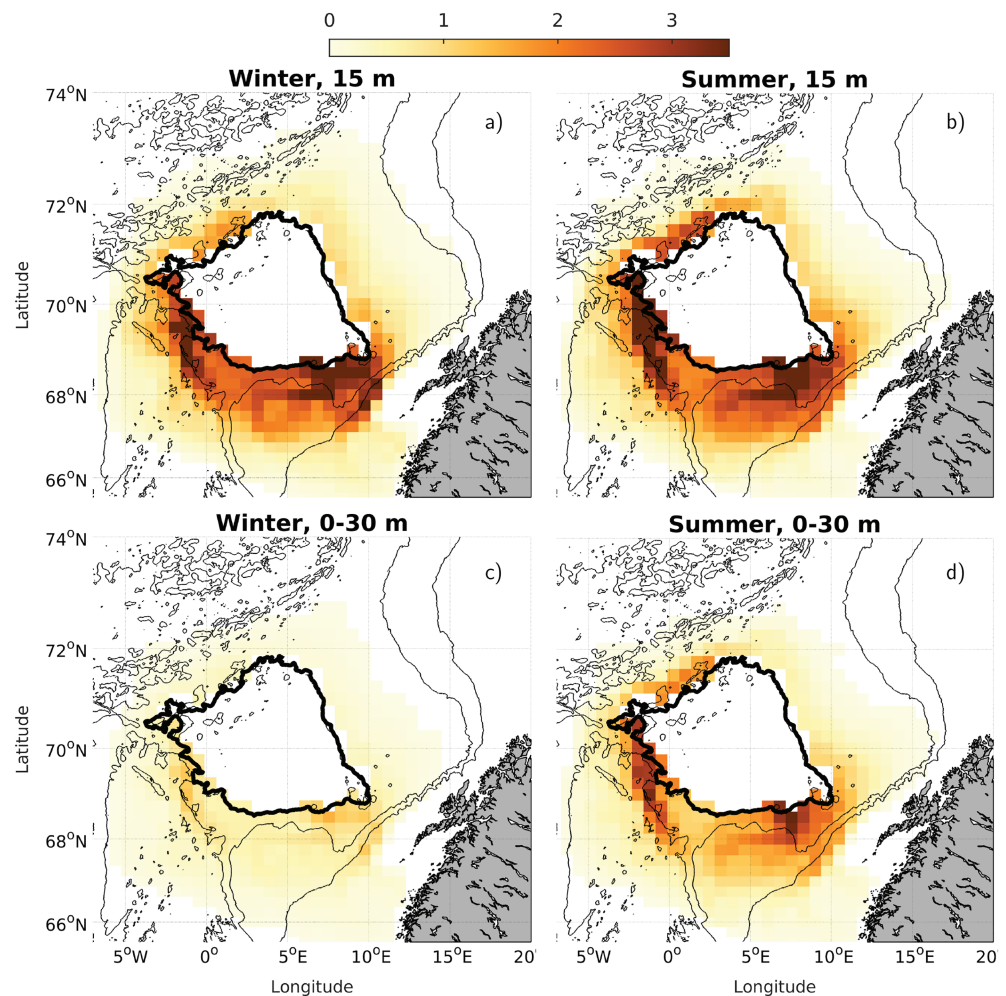
Figure 6. Density maps of (a and b) 2-D drifters at 15-m depth and (c and d) 3-D drifters deployed at 15 m entering the LB between 0- and 30-m depth in winter (January–March, left panels) and summer (July–September, right panels). Only trajectory segments from deployment until the longest stay entry are considered. Color bars show the percentage of drifters in a bin normalized with the total number of drifters entering the LB for the given deployment depth (2-D 15 m: 60,432; 3-D 15 m: 61,730). Bin sizes are as in Figure 3.

vice versa for Depth Class 2. Specifically, we estimate that among the drifters in Depth Class 1, about 28% enter the basin during summer and about 22% enter the basin during winter. Furthermore, we observe that during summer, the relative amount of drifters in Depth Class 1 that are deployed at 15 m is larger than during winter (82% vs. 62%). This is mainly because the drifters deployed at 15 m can sink in winter (to Depth Class 2) while they remain in Depth Class 1 during summer.

The density maps of drifters in the three depth classes (0–130 m, 130–370 m, and 370 m-bottom) are shown in Figure 5 for trajectory segments between deployment and the longest stay entry. The color bar indicates the percentage of drifters in a bin when normalized by the total number of drifters in all depth classes in order to better visualize the seasonal-vertical variations of the inflow to the LB. The seasonal behavior shows up in Figures 5a–5d as stronger colors (larger percentages) in panel b compared to panel a and also to some extent stronger colors in panel c compared to panel d. Note that the seasonal variability is stronger in Depth Class 1, nearby the surface where the atmospheric cooling/warming largely affects the stratification of the water column. For Depth Class 3, at depths below 370 m, (Figures 5e and 5f) the synthetic drifter densities and patterns show only weak seasonal variation.

Despite the seasonal variations in the density maps, the main inflow pathways toward the basin are similar. For Depth Classes 1 and 2 the LSI and HI are pronounced in both seasons. For Depth Class 3 we also observe these features, but in the east toward the continental slope, we also notice enhanced drifter densities around

Table 2
Percentages of Synthetic Drifters (2-D and 3-D Lagrangian Experiments) Classified According to the Temperature Loss in the LB During Their Longest Stay in the Basin

Depth/depth class	1 <−1 ° C [%]	2 −1–0 ° C [%]	3 0–1 ° C [%]	4 >1 ° C [%]
2-D				
15 m	7	13	8	4
200 m	5	15	13	2
500 m	3	11	11	3
3-D				
(0–130 m)	8	14	10	3
(130–370 m)	2	14	12	1
(370 m-bottom)	1	16	14	0

Note. Temperature Class 1 (drifters that experience more than 1 ° C cooling), Temperature Class 2 (between 0 and 1 ° C cooling), Temperature Class 3 (between 0 and 1 ° C warming), and Temperature Class 4 (more than 1 ° C warming). Listed are percentages of drifters deployed at 15-, 200-, and 500-m depths (2-D) and drifters belonging to Depth Classes 1, 2, and 3 (3-D) that belonged to the given temperature class. The percentages are computed by normalizing by the number of drifters entering the LB independent on deployment level/depth class (2-D: 60,432 + 61,841 + 53,603 = 175,884 drifters; 3-D: 62,355 + 51,915 + 63,661 = 177,931 drifters).

larger stretches of the basin boundary. We take this as indication of enhanced topographic steering of flow (and drifters) at depth.

3.4. Two-Dimensional Versus Three-Dimensional Lagrangian Trajectories

We assess the differences between the 2-D and 3-D simulations in terms of the near-surface circulation where the vertical displacements and seasonality are more pronounced (Figure 6). We show winter (left panels) and summer (right panels) density maps for the 2-D synthetic drifters at 15 m (top panels) and the 3-D synthetic drifters deployed at 15 m and entering the LB at the depth of 0–30 m (15 m ± 15 m, bottom panels). The maps reveal that the seasonality in drifter distributions is much more pronounced for the 3-D synthetic drifters than for the 2-D synthetic drifters. For instance, the percentage of 3-D drifters that enter the basin in winter versus summer between 0- and 30-m depth, when normalized to the amount of 3-D drifters deployed at 15 m that entered the LB (Table 1), is 8% and 20%, respectively. This strong seasonality is again coupled to the vertical structure of the inflow: During winter (panel c), the 3-D drifters have sunk below our defined depth range, and as a consequence, they have lower occurrence density than in summer (panel d), consistent with our interpretation of results shown in the previous section. For the 2-D drifters, the drifter densities in different seasons can only be affected by a change of pathways between summer and winter that would make the amount of drifters entering the basin at the given depth to change between the seasons. However, the drifter densities between winter and summer are similar (Figures 6a and 6b), and the two seasons account for approximately the same percentage of drifters entering the basin (winter: 24%, summer: 25%) when normalized against the amount of 2-D drifters entering the basin when deployed at 15 m (Table 1), indicating a strong difference between the 2-D and 3-D drifters.

A similar comparison of the 2-D and 3-D drifters deployed at 200- and 500-m depths (not shown) reveals seasonal differences, but with smaller amplitude at 200 m and hardly discernible at 500 m. This result is consistent with Figures 5e and 5f for Depth Class 3, indicating similar drifter densities and patterns in the two panels, implying that the seasonal variation in vertical displacement of the drifters is small when we integrate the drifter densities over the water column below 370-m depth.

3.5. Implications for Heat Exchange

As seen from Figure 5 and mentioned in section 3.3, the inflows to the LB preferentially come more from the slope at deeper levels compared to the surface. It is of interest to see whether this has an impact on the AW-LB heat exchange. As a proxy to quantify the heat exchange associated with the inflow, we study pathways toward the LB of synthetic drifters that experience a certain temperature change within the basin. We thereby assume that the temperature change occurs along the drifter trajectory (see section 4.3 for further discussion). Because several previous studies used 2-D surface drifters and RAFOS floats to study the heat
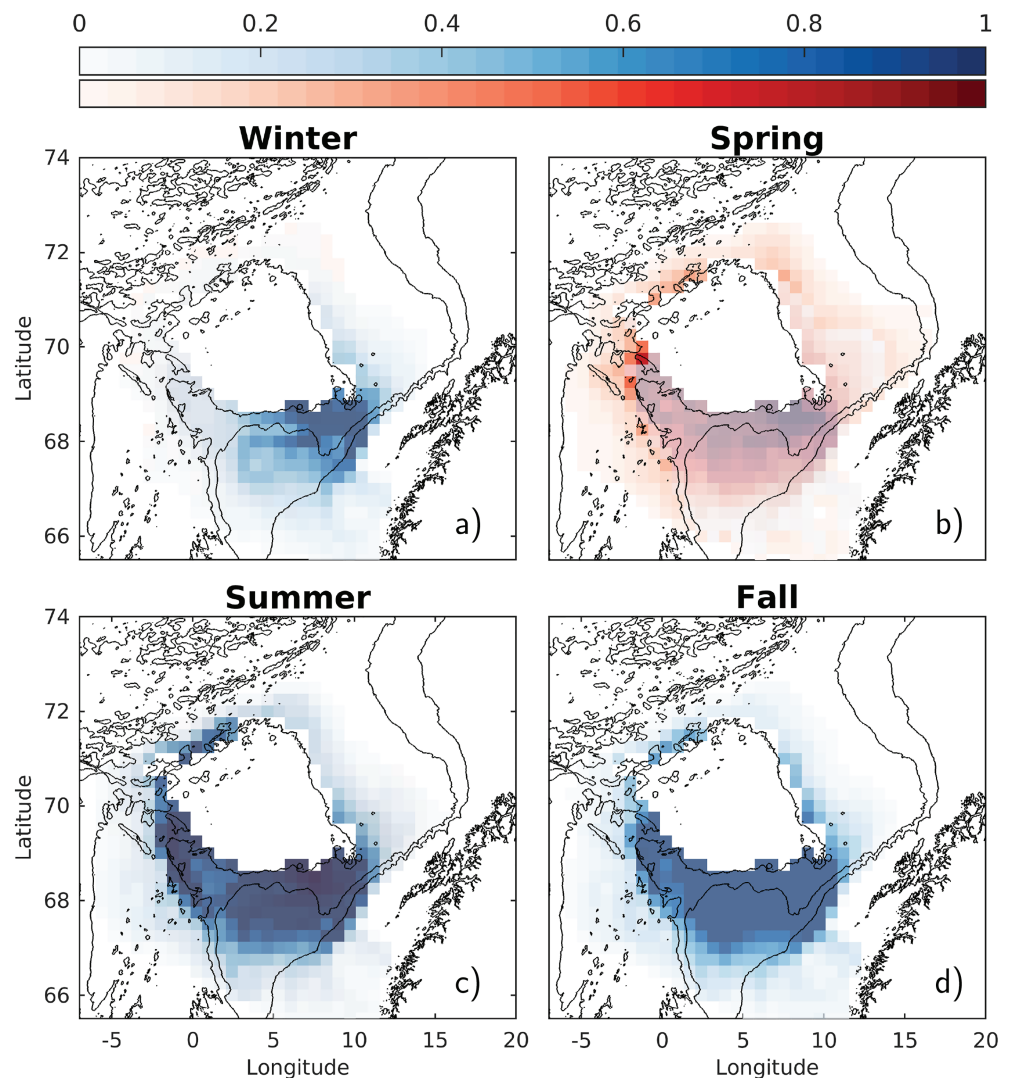
Figure 7. Drifter density maps of 3-D drifters in Depth Class 1 (0–130 m) that belonged to (blue colors) Temperature Class 1 (cooling more than 1 ° C in the LB) and (red colors) Temperature Class 4 (warming more than 1 ° C in the LB) subsampled by the season of the longest stay entry to the LB. Only trajectory segments from deployment until the longest stay entry are considered. Color bars show the percentage of drifters in each bin relative to the total number of 3-D drifters belonging to Depth Class 1 (62,355 drifters). Since the color maps can overlap, blue colors are mapped over red colors using 30% transparency. Bin sizes are as in Figure 3.

exchange (Dugstad et al., 2019; Isachsen et al., 2012; Koszalka et al., 2013; Rossby et al., 2009), we also investigate the differences between the 2-D Lagrangian simulations (synthetic drifters are fixed at their respective deployment depths) and 3-D Lagrangian simulations (where we apply the entry depth classes defined in section 3.3).

Similar to the analysis in Dugstad et al. (2019), we quantify the temperature change during the longest stay in the LB for each synthetic drifter by calculating the temperature change between the entry and the exit of this stay: $\Delta T = T_{exit} - T_{entry}$, where T_{exit} and T_{entry} are the synthetic drifter temperatures at the longest stay exit point and longest stay entry point, respectively. Because we require that a synthetic drifter exits the basin, trajectory segments that terminate their lifetime inside the basin are excluded from the analysis. Due to generally short residence times at the surface and slightly longer at deeper levels, this affects only a small percentage of trajectories that increases at deeper levels: for the 2-D drifters, 0% (15 m), 3% (200m), and 9% (500 m) and for the 3-D drifters, 1% (Depth Class 1), 4% (Depth Class 2), and 12% (Depth Class 3).

Based on ΔT, we define four temperature classes: (1) drifters that cooled by more than 1 ° C; (2) cooled by 0–1 ° C; (3) warmed by 0–1 ° C; and (4) warmed by more than 1 ° C. The percentages of drifters in

each temperature class normalized with respect to all drifters that entered the LB summed over deployment depths (2-D = 175,884 drifters) or depth classes (3-D = 177,931 drifters) are given in Table 2. Note that the percentages do not sum up to 100, because the drifters terminated in the basin were not taken into account. In general, for both 2-D and 3-D drifters more drifters are cooled in the basin than warmed, implying a net heat loss in the basin for the drifters that enter. About 54% (55%) of the 2-D (3-D) drifters experienced cooling in the basin and 41% (40%) of the 2-D (3-D) drifters experienced warming (the rest ended their lifetime in the basin). In Temperature Class 1 with largest temperature loss, water parcels associated with drifters deployed at 15-m depth give the largest contributions to the heat loss in the basin (Table 2). However, drifters at deeper levels also indicate significant contribution to the heat loss. We note that the relative amount of drifters in Temperature Class 1 is larger than the amount of drifters in Temperature Class 4 (possibly with the exception of drifters at the deepest levels), indicating a net temperature loss in the LB. This is consistent with a net surface heat loss in the basin of 5.2 TW that was estimated by Dugstad et al. (2019) from a ROMS model with 4-km grid resolution when averaged between 1997 and 2005. Surface heat fluxes were unfortunately not saved from our model runs, but the drifter results are consistent with direct estimates of the lateral heat transport into the LB. Using model velocity and temperature fields from January 1996 to January 2000, we found a net advective heat transport convergence of 12 TW in the basin. The gap between this result and the surface heat loss estimated by Dugstad et al. (2019) is likely due to the different model configurations (e.g., resolution) and that the averaging is done over different time periods.

We construct synthetic drifter density maps of Temperature Classes 1 and 4 divided in four seasons: January–March, April–June, July–September, and October–December. The density maps for 3-D drifters in Depth Class 1 from deployment until their longest stay entry are shown in Figure 7 (2-D drifters deployed at 15 m have very similar patterns and seasonal variations and are therefore not shown). Synthetic drifters that enter the basin during late summer and fall mainly cool (blue shades) while those entering in late spring (April–June) experience warming (red shades) in the basin where they spend the following summer months. Late winter entries also experience cooling, in particular from the LSI. In late summer and early winter, drifter entries along the entire southern LB boundary experience cooling. This is consistent with Dugstad et al. (2019), who showed that the surface water masses with the largest temperature decrease in the LB entered the LB as a slab from the south.

The results for the 2-D synthetic drifters deployed at 500 m (Figure 8) can be compared to the 3-D drifters in Depth Class 3 (depths larger than 370 m; Figure 9). Note that the relative contribution at these levels are larger for the 2-D drifters than the 3-D drifters (Table 2). Therefore, the color scale is different in Figures 8 and 9 (discussed further in section 4.2). The general pathways, without taking seasonality into consideration, are similar in the 2-D and 3-D simulations with a cooling pronounced for the entries from the east and warming for entries from the west. Unlike at the surface (cf. Figure 7), the drifter density associated with cooling along the southern boundary of the basin is less pronounced, and instead, the inflows from the LSI and HI regions appear more important: LSI for the cooling of the warm AW entering from the east and HI for the warming of the colder waters from the FC, especially for the 2-D drifters (Figure 8). Seasonal variations are more pronounced in the 3-D drifters (Figure 9). Notably, there are approximately two times more 3-D drifters in Temperature Class 1 (cooling) that enter the basin during winter (January–March) than the other seasons. In winter the drifters that are cooled enter the basin from all sides, implying that the associated water masses are affected by the atmospheric cooling regardless of their entry region. We also notice that the cooling at deeper levels is delayed compared to near the surface (Figure 7) where the drifters experienced intense cooling in July–December. Largest warming (strong red colors) is seen in spring (Figure 9b), likely related to atmospheric warming. Summer and fall patterns are similar and resemble those for the 2-D drifters showing the cooling from the LSI and warming from the HI.

4. Discussion
4.1. Effects of Dynamics and Residence Times in the Basin
Our analyses show that the drifters entered the LB via two main routes, the LSI and the HI. While we have primarily focused on the inflow to the LB, the dynamics inside the LB is also of importance for the modification of the water parcels entering the basin, particularly by affecting the residence times in the basin (Table 1). In Figure 10, we show density maps similar to Figure 5, but now for the full trajectories including the trajectory segments in the basin. Superimposed binned velocity fields estimated from the same drifter data show a large cyclonic circulation around the basin, consistent with Volkov et al. (2013). Many of the HI
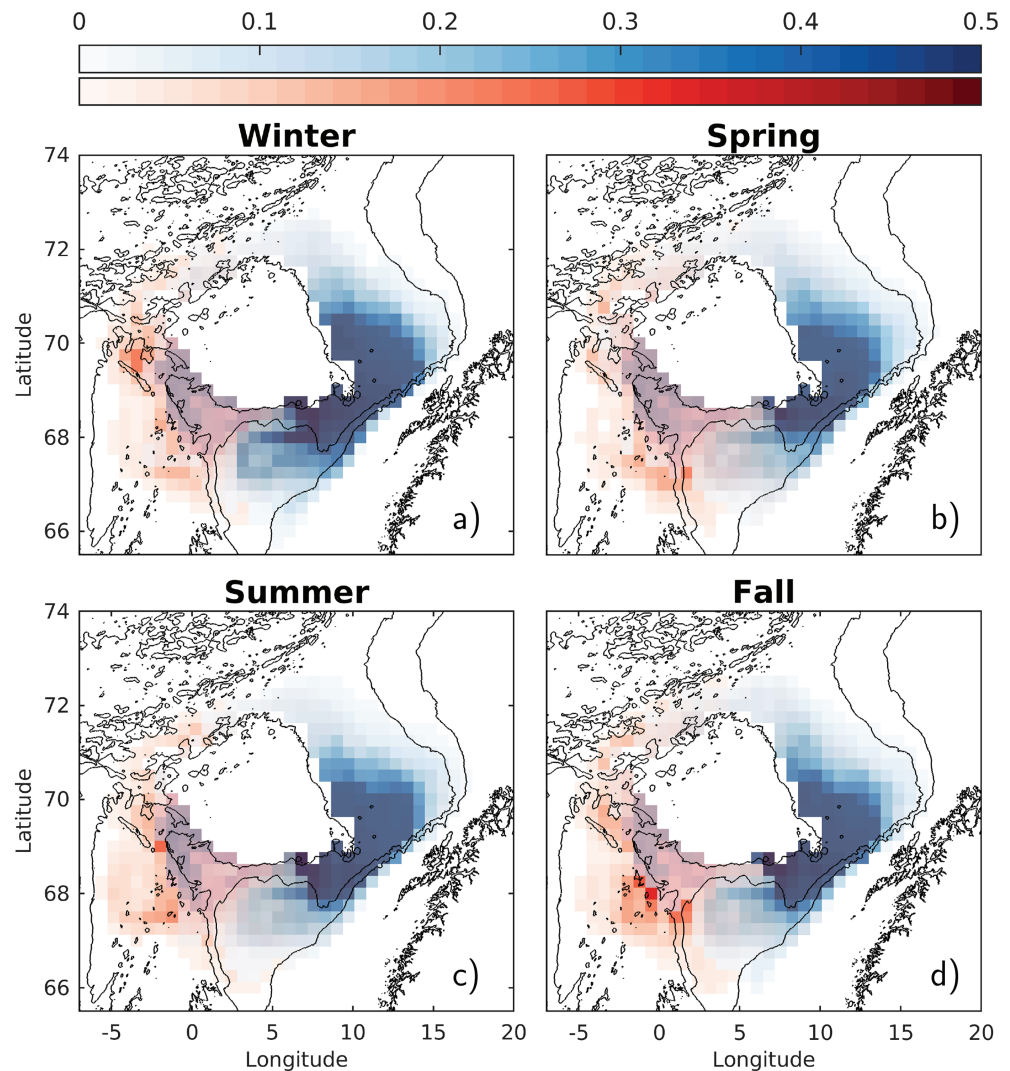
Figure 8. Drifter density maps of 2-D drifters deployed at 500-m depth that belonged to (blue colors) Temperature Class 1 (cooling more than 1 ° C in the LB) and (red colors) Temperature Class 4 (warming more than 1 ° C in the LB) subsampled by the season of the longest stay entry to the LB. Only trajectory segments from deployment until the longest stay entry to the basin are considered. Color bars show the percentage of drifters in each bin relative to the total number of 2-D drifters entering the LB when deployed at 500-m level (53,603 drifters). Since the color maps can overlap, blue colors are mapped over red colors using 30% transparency. Bin sizes are as in Figure 3.

drifters, that is drifters that entered the LB through the HI, follow this pattern and travel a comparatively long distance in the basin, which likely increases their residence times. As mentioned in section 3.2 the occurrence density of HI drifters increases with depth. Furthermore, since the residence times inside the basin are longer for HI drifters, this region appear to be an important route for the water that is warmed in the basin.

The percentages reported in section 3.2 indicated that the relative amount of drifters entering the LB via the LSI were almost constant with depth, but for the HI the relative amount of drifters increased from 17 to 25% for drifters deployed at 15 and 500 m, respectively. The HI is concentrated in the region where the LB contour do not close originally. Isachsen et al. (2003) and Nøst and Isachsen (2003) showed that the currents in the Nordic Seas follow the topography. Hence, as the 3,000-m isobath near the HI turns eastward and along the northern rim of the Vøring Plateau, the drifters could experience this topographical steering and veer eastward into the basin. The velocity vectors in Figure 10 support this. While the variability in wind and stratification would disturb topographical steering in upper layers (e.g., for deployments at 15- and 200-m depth), their influence diminish with depth. The drifters deployed at 500 m would feel strong topographic
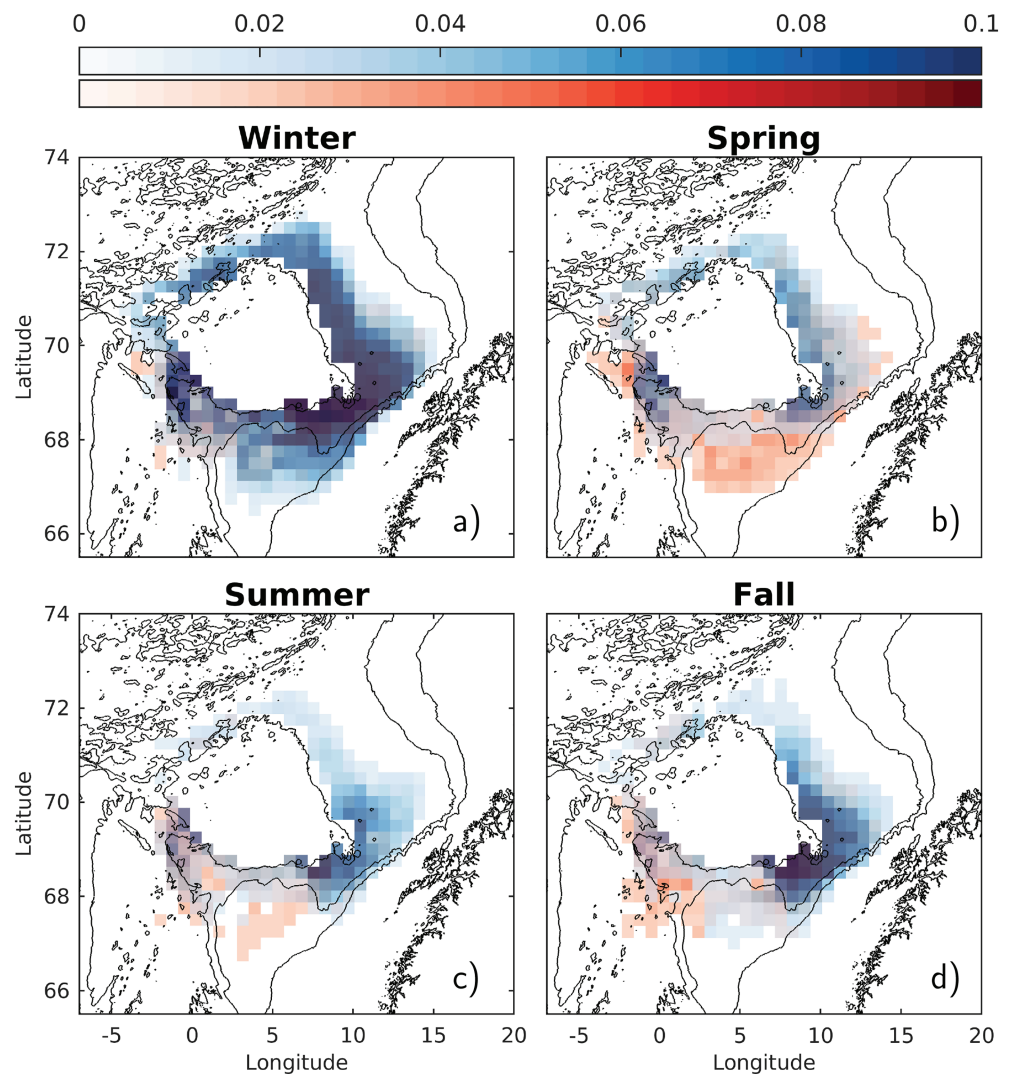
Figure 9. Drifter density maps of 3-D drifters in Depth Class 3 (370 m-bottom) that belonged to (blue colors) Temperature Class 1 (cooling more than 1 ° C in the LB) and (red colors) Temperature Class 4 (warming more than 1 °C in the LB) subsampled by the season of the longest stay entry to the LB. Only trajectory segments from deployment until the longest stay entry to the basin are considered. Color bars show the percentage of drifters in each bin relative to the total number of 3-D drifters in Depth Class 3 (63,661 drifters). Since the color maps can overlap, blue colors are mapped over red colors with 30% transparency. Bin sizes are as in Figure 3.

potential vorticity gradients and remain locked to topography, leading to larger percentages of entry via the HI compared to near the surface.

Inside the LB, the velocity fields revealed the anticyclonic structure of the Lofoten Basin Eddy (LBE) in the center (Ivanov & Korablev, 1995; Fer et al., 2018). The location of this large vortex is close to the Helgeland Ridge. The retention by the eddy is expected to increase the residence time in the basin, particularly for the HI entries. In addition to the LBE, the velocity fields indicated surface-intensified anticylonic structures close to the LSI at the edge of the basin contour. These anticyclonic circulations can have consequences for the residence time of the LSI entries, for example, lead to a relatively rapid exit from the LB in this region and fairly short residence times for the LSI drifters in the LB compared to the HI drifters. The EKE map from the ROMS model (averaged between 1996 and 1999, not shown) identified this region as a secondary EKE maximum (in addition to the LBE). This is consistent with the satellite-derived EKE observations reported in Isachsen et al. (2012), surface drifter trajectories shown by Koszalka et al. (2011), and with the eddy census from altimeter data and surface drifters by Raj et al. (2016). The LSI as an eddy hot spot is further supported by a local deepening of time-averaged potential density surfaces there. For example, the $\sigma_0 = 27.9$ kg/m^3
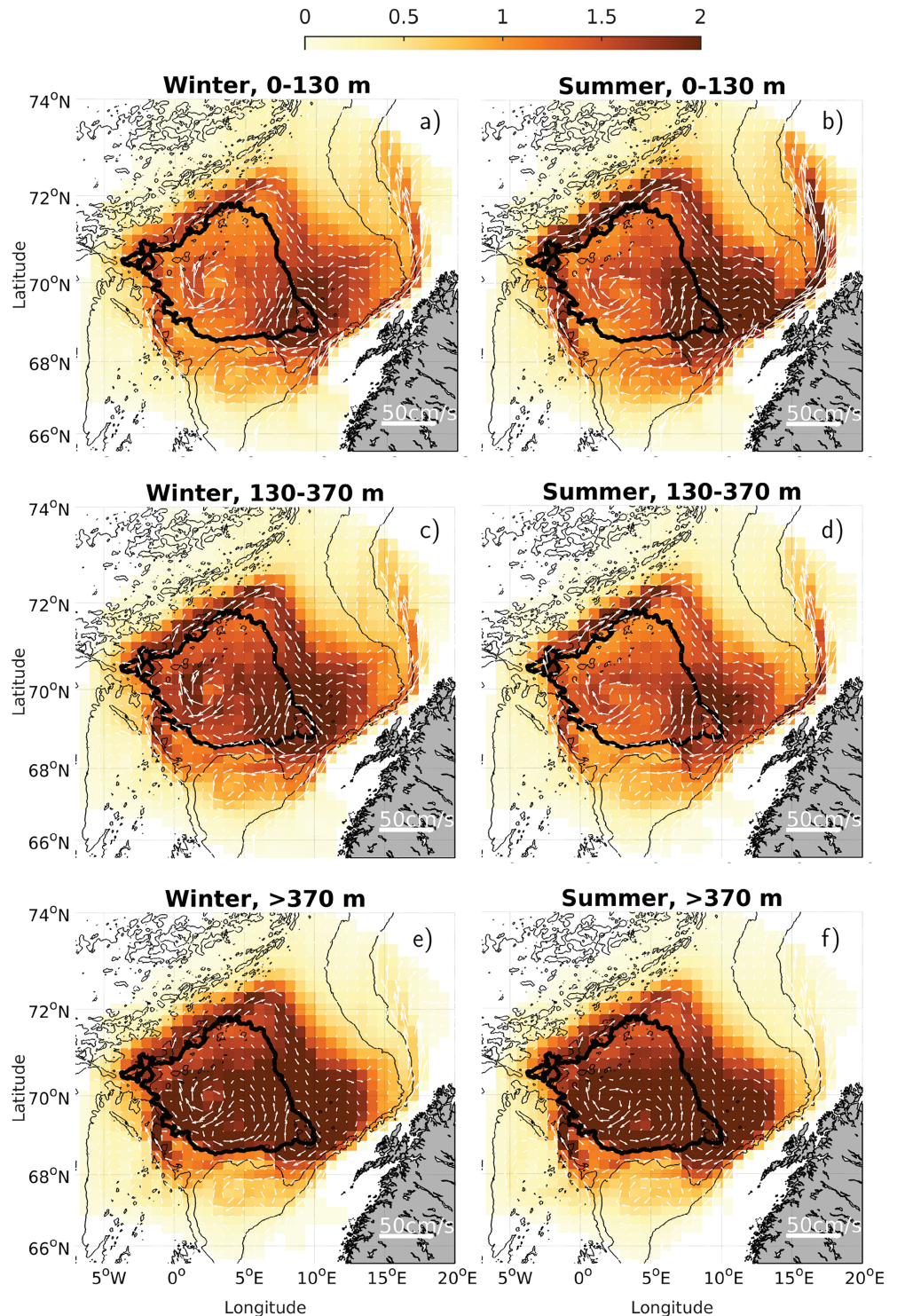
Figure 10. Density maps of 3-D synthetic drifters entering the LB in different seasons, (a, c, and e) January–March and (b, d, and f) July–September, and at different depths. We consider the longest stay entry to define the depth classes 1:0–130 m (a,b), 2:130–370 m (c,d) and 3:370 m–bottom (e,f). Thus, density maps are similar to Figure 5, but here we analyze full trajectories. The color bar shows the percentage of drifters when normalized with the total number of drifters entering the basin summed over depth classes (62,355 + 51,915 + 63,661 = 177,931). Superimposed are the corresponding velocity vectors binned from drifter velocities. Bin sizes are as in Figure 3 and are the same for the drifter density and the velocity fields.

surface reached 600-m depth in the LSI region, approximately the same as in the LB center, consistent with Rossby et al. (2009) and Richards and Straneo (2015). The mean temperature at 200 m was also higher at the LSI compared to the basin (Figure 1b), implying retention of warm water close to the LSI. Because of the on average warm temperature signal in the LSI region, the winter cooling was also more intense there, resulting in larger vertical displacements than in the HI during winter (Figure 4b).

We observe generally higher drifter densities in the basin at deeper levels (Figures 10e and 10f). Drifters at deeper levels from the LSI are advected farther into the basin compared to the surface, suggesting decreased residence times for the 15- and 200-m LSI drifters as a result of the secondary EKE maximum. The increased residence time at depth together with deep-reaching warm water in the LSI compared to surroundings contributes to the strong cooling of water masses entering the LB from the slope via the LSI (Figures 8 and 9).

4.2. Missing Structure and Variability in 2-D Analyses and Observations

The warm Atlantic inflow to the LB exhibits seasonal variability related to changes in atmospheric forcing and the resulting sinking and mixed layer depth evolution. During winter, the 3-D synthetic drifters experience larger vertical displacements (causing the redistribution of the drifters in the vertical), while during summer, the strong stratification restrict the drifters to their deployment level. The seasonal differences are stronger at the surface and less pronounced at depth and lead to differences in the vertical distributions of the synthetic drifters in the 2-D and 3-D simulations, in particular at the surface layer. The combined vertical-seasonal variations of the inflow have consequences for the heat exchange between the AW inflow and the LB.

The seasonal signal at deeper levels in the 3-D drifters was more pronounced than in the 2-D drifters. Half of the 3-D drifters in Temperature Class 1 and Depth Class 3 entered the basin at depths shallower than 500 m. Therefore, they were more likely to be affected by seasonal variations in contrast to the 2-D drifters fixed at 500-m depth. For this reason, deep drifters that are cooled could enter the basin from many regions in winter, but those that experience warming entered typically from south during spring. Another important difference between the 2-D and 3-D drifters is that the number of drifters in Temperature Classes 1 and 4 at deeper levels were substantially less for 3-D drifters (Table 2). While the 2-D drifters are fixed in depth, we observed differences in the depth of entry for the different temperature classes in the 3-D drifters. The majority of 3-D drifters sunk toward the basin (Figure 4), and the median depth of entry for drifters in Depth Class 3 was 545 m. The sinking was also reflected in the temperature classes. The entry median depth for the largest temperature change classes (1 and 4) was about 500 m. These depths are at the base of the Atlantic layer, and the sinking therefore has a large impact on the temperature changes in the basin. The majority of drifters sunk below the Atlantic layer where the water masses are more uniform. The vertically rigid 2-D drifters therefore likely overestimate the temperature changes.

Some important implications of our results thus emerge regarding real Lagrangian observations. Several previous studies have used 2-D surface drifters anchored at 15-m depth and equipped with a temperature sensor to study the AW inflow in the Nordic Seas and its seasonal or winter expression (Andersson et al., 2011; Isachsen et al., 2012; Koszalka et al., 2013; Poulain et al., 1996). Our results suggest that such surface drifters must be used with caution. They do not correctly represent seasonal variations in the surface inflow, which is affected by winter cooling and sinking and then summer warming and restratification (Figures 5 and 6). Furthermore, as the 3-D synthetic drifters also indicate a net sinking toward the LB (Figure 4a), the surface drifters that are anchored at a given depth may give a wrong representation of the water mass characteristics (i.e., salinity and temperature) with time since they do not capture the changes associated with the vertical motion. Our results also suggest that surface drifters alone cannot be used to accurately study the inflow and associated heat exchange because of the variations in the vertical structure of the inflow. To this end, the subsurface floats should complement the surface drifters, as was already pointed out by Rossby et al. (2009). However, due to instrument and deployment costs and technical challenges, there are very few (~20) subsurface float observations in the eastern Nordic Seas and the LB. The observations are too few to provide a basis for the statistical evaluation of our Lagrangian simulations. Furthermore, the subsurface floats that have been used previously in the Nordic Seas are mainly isobaric and thus cannot capture vertical motions, for example, the net sinking experienced by water parcels. Isopycnal floats exist and can to some extent move in the vertical. But by tending to follow isopycnals, they are ill-suited for detecting the diabatic transformations experienced by water parcels. Development of an affordable subsurface float technology that would allow numerous deployments and provide a more realistic measure of the vertical motion

is therefore a priority. Such observations would be invaluable in studying the cooling and sinking processes in the LB, and water mass transformation processes in general. Lacking the observation technology, studies using fully 3-D synthetic drifters serve as a good complement to the already existing Lagrangian field observations.

4.3. Limitations of Our Approach

Our results about the vertical structure and seasonal variations of the inflow are generally consistent with previous studies based on observations and Eulerian modeling (Dugstad et al., 2019; Isachsen et al., 2012; Rossby et al., 2009). However, our study is the first to study the inflow to the LB using 2-D and 3-D Lagrangian simulations based on a high-resolution ocean model.

The relative dispersion statistics from the 2-D Lagrangian simulations at 15 m compared very well with the surface drifter observations, giving confidence on the ability of the ocean model and the Lagrangian model to simulate the near-surface flows. A statistical comparison with observations at deeper levels was not possible because of too few float data. Since computations at deeper levels are based on similar methods, we assumed that drifters at these levels were able to represent the associated flows. The 2-D and 3-D simulations agreed well in pathways and statistics of drifters interacting with the LB and residence time analysis in the basin. We interpreted this as an indication that the 3-D drifters were physically meaningful. Furthermore, the 3-D drifters showed intuitive results, for instance that they moved more freely in the vertical when the stratification was weak and that they were trapped closer to their deployment depth when the stratification was stronger. We therefore have confidence in the 3-D drifters, and, together with the 2-D drifters, the analyzed trajectories can be used to study our earlier defined research problems.

In assessing our results pertaining to vertical motions, one has to bear in mind that the ROMS model used here is hydrostatic and hence does not reproduce convection processes occurring in the LB exactly, but merely parameterizes them. So the results shown and discussed here are related to large-scale and mesoscale flow features rather than to small-scale mixing processes. Although the $k - \epsilon$ vertical mixing scheme applied here has been shown to compare favorably with laboratory experiments (Warner et al., 2005), errors in the mixing scheme can be expected to impact our model predictions, including the resolved vertical flow field. However, mixing-related errors in the model's vertical velocities cannot be too large since the vertical velocities are also constrained by the topographically guided horizontal flow via the continuity equation. Most of our findings regarding vertical motions are also very clear and intuitive. There is a strong distinction in vertical displacements between summer and winter, and there is strong evidence of a net sinking in the LB region with time, consistent with the on average large surface heat and buoyancy loss there (Richards & Straneo, 2015). A closer investigation into the effects of various choices for the vertical parameterization schemes is beyond the scope of this study. And, as argued, the core features seen herein are likely fairly robust to such choices.

The ability of off-line Lagrangian simulations in representing the parameterized vertical diffusion present in the ROMS model can also be questioned. However, for a model output of high-resolution and high output frequency as used here, it is customary not to include additional diffusion; see, for example, Bower et al. (2011), Gelderloos et al. (2017), Rühs et al. (2019), and Dugstad et al. (2019). This is because the dominant turbulent (nonlocal) transport by ocean eddies is resolved and the local small-scale mixing is small in comparison. Adding vertical diffusion (parameterized as random walk for the synthetic drifters) could lead to distorting of the synthetic drifter spreading and make the Lagrangian simulations too diffusive and thus inconsistent with the Eulerian ocean model used to force them. The inclusion of vertical diffusion (as well as lateral diffusion) in Lagrangian models must address a proper choice of the stochastic model and its coefficients with respect to the unresolved nonlocal mixing, boundary effects, and spatially variable diffusivity; see, for example, Hunter et al. (1993), Griffa (1996), and Berloff and McWilliams (2002). In a recent study, Wagner et al. (2019) evaluated the ability of off-line Lagrangian simulations to reproduce spreading of a tracer patch simulated in-line with the advection diffusion equation of the ocean model. They used a daily output of a high-resolution model and a vertical diffusivity coefficient varying by 5 orders of magnitude with depth and seasonally. The detected differences in vertical spreading were small and attributed to daily averaging of the model output and the depth variations in the vertical diffusivity. The model output in our case is four times as frequent (for comparable Lagrangian integral time scale in both regions), which further enhances ability of our Lagrangian model to represent transport processes. However, if we were to

add an unknown yet realistic value of vertical spreading, it would not change the general conclusions from our study but rather enhance the differences between the 2-D and 3-D simulations.

Throughout our discussion regarding temperature changes in the basin, we have used terminology such as "AW-LB heat exchange" and that "drifters can experience cooling." These statements assume that the synthetic drifters represent actual water parcels accurately and that the temperature changes occur along the drifter trajectories. This common assumption can be questioned, as there are no actual measurements on how "Lagrangian" a synthetic drifter or an observed drifter/float is. Especially, since observed drifters/floats are 2-D, they only follow the horizontal components of the flow that can result in errors. However, given that the vertical shear is weak, one can assert that they represent the water masses quite well (LaCasce, 2008; Rossby et al., 2009). The synthetic drifters, and especially the 3-D drifters, can even better represent the trajectory of a water parcel than the observations. They are advected by Lagrangian equations and are therefore purely Lagrangian, with the exception of small numerical errors and uncertainties.

5. Summary and Conclusions

We have studied the AW inflow to the LB by analyzing 2-D (fixed depth) as well as fully 3-D Lagrangian trajectories of synthetic drifters advected by currents from a high-resolution ocean model of the region. Synthetic drifters deployed at three levels (15, 200, and 500 m) were used to deduce the main inflow pathways of AW into the basin, including the vertical structure of the inflow and its seasonal variations. We inferred patterns of heat exchange associated with the inflow at different depths and seasons.

The 2-D Lagrangian simulations at 15 m were compared to surface drifter observations in terms of relative dispersion statistics, showing a close agreement. This gave confidence to the ability of the ocean model and the Lagrangian model to simulate the near-surface flows.

A large percentage of the inflow to the LB (about 50% synthetic drifters at all depths) was concentrated in two regions: one to the east, at the slope close to the Lofoten Islands (LSI), and one to the west, close to the Helgeland Ridge (HI). The mean residence time in the LB increased with depth as the drifters at deeper levels were advected further into the basin compared to drifters near the surface.

The inflow at different depths exhibited seasonal variability, which was most pronounced in the east (LSI). These seasonal differences were stronger at the surface where they led to differences in the distributions of the synthetic drifters in the 2-D and 3-D simulations.

The combined vertical-seasonal variations of the inflow affected the inferred heat exchange between the AW inflow and the LB in the surface layer. The strongest cooling in the LB was experienced by synthetic drifters entering from a broad southern region and was intensified in winter. In late winter the cooling was experienced mostly by the drifters entering from the southeast, through the LSI. During the summer, the synthetic drifters in the surface layer experienced a seasonal warming. This pattern in the near-surface layer was similar in the 2-D and 3-D drifter simulations.

The pattern of the temperature change was different in deeper layers where the 2-D and 3-D simulations also differed. However, the general pathways were quite similar in the two simulations, showing that the cooling was mainly experienced by the warm AW inflow entering from the east (LSI) while the synthetic drifters entering via HI in the west tracked the colder waters of the FC. The 2-D simulations did not capture the seasonal variations at 500 m, but they were pronounced in the 3-D simulations. We explained the differences by the vertical sinking of the 3-D drifters. The drifters that experienced seasonality typically entered the basin at levels shallower than 500 m. However, because the majority of 3-D drifters entered the basin below the base of the Atlantic layer, we found fewer 3-D drifters that experienced large cooling/warming at deeper levels compared to the 2-D drifters at 500-m depth.

Our results suggest that surface drifters must be used with caution, as they might give wrong representations of the seasonal variations in the surface inflow, which is affected by winter cooling and sinking, and summer warming and restratification. The temperature and salinity changes associated with the vertical movements and the variations in the vertical structure of the inflow are not captured by the 2-D synthetic drifters or the surface drifters anchored at a given depth. Lacking the observation technology that can represent the vertical motion associated with water mass transformations, statistical analysis of a large number of 3-D synthetic drifters from high-resolution Lagrangian simulations provides insight.

References

Andersson, M., Orvik, K. A., Lacasce, J. H., Koszalka, I., & Mauritzen, C. (2011). Variability of the Norwegian Atlantic Current and associated eddy field from surface drifters. *Journal of Geophysical Research*, *116*, C08032. https://doi.org/10.1029/2011JC007078

Årthun, M., Bogstad, B., Daewel, U., Keenlyside, N., Sando, A., & Schrum, C. (2018). Climate based multi-year predictions of the Barents Sea cod stock. *PLoS ONE*, *13*(10), e0206319. https://doi.org/https://doi.org/10.1371/journal.pone.0206319

Årthun, M., Eldevik, T., & Smedsrud, L. H. (2019). The role of Atlantic heat transport in future Arctic winter sea ice loss. *Journal of Climate*, *32*(11), 3327–3341. https://doi.org/10.1175/JCLI-D-18-0750.1

Berloff, P. S., & McWilliams, J. C. (2002). Material transport in oceanic gyres. Part II: Hierarchy of stochastic models. *Journal of Physical Oceanography*, *32*(3), 797–830.

Bosse, A., Fer, I., Søiland, H., & Rossby, T. (2018). Atlantic Water transformation along its poleward pathway across the Nordic Seas. *Journal of Geophysical Research: Oceans*, *123*, 6428–6448. https://doi.org/10.1029/2018JC014147

Bower, A., Lozier, M., & Gary, S. (2011). Export of Labrador Sea Water from the subpolar North Atlantic: A Lagrangian perspective. *Deep Sea Research Part II: Topical Studies in Oceanography*, *58*, 1798–1818. https://doi.org/10.1016/j.dsr2.2010.10.060

Dagestad, K. F., Röhrs, J., Breivik, O., & Ådlandsvik, B. (2018). OpenDrift v1.0: A generic framework for trajectory modelling. *Geoscientific Model Development*, *11*(4), 1405–1420. https://doi.org/10.5194/gmd-11-1405-2018

Dagestad, K. F., & Röhrs, J. (2019). Prediction of ocean surface trajectories using satellite derived vs. modeled ocean currents. *Remote Sensing of Environment*, *223*, 130–142. https://doi.org/10.1016/j.rse.2019.01.001

Dee, D. P., Uppala, S. M., Simmons, A. J., Berrisford, P., Poli, P., Kobayashi, S., & Vitart, F. (2011). The ERA-Interim reanalysis: Configuration and performance of the data assimilation system. *Quarterly Journal of the Royal Meteorological Society*, *137*(656), 553–597. https://doi.org/10.1002/qj.828

Dugstad, J., Fer, I., LaCasce, J. H., Sanchez de La Lama, M., & Trodahl, M. (2019). Lateral heat transport in the Lofoten Basin: Near-surface pathways and subsurface exchange. *Journal of Geophysical Research: Oceans*, *124*, 2992–3006. https://doi.org/10.1029/2018JC014774

Fer, I., Bosse, A., Ferron, B., & Bouruet-Aubertot, P. (2018). The dissipation of kinetic energy in the Lofoten Basin Eddy. *Journal of Physical Oceanography*, *48*, 1299–1316. https://doi.org/10.1175/JPO-D-17-0244.1

Gelderloos, R., Haine, T. W. N., Koszalka, I., & Magaldi, M. (2017). Seasonal variability in warm-water inflow towards Kangerdlugssuaq Fjord. *Journal of Physical Oceanography*, *7*(47), 1685–1699. https://doi.org/10.1175/JPO-D-16-0202.1

Griffa, A. (1996). Applications of stochastic particle models to oceanographic problems. In R. J. Adler, P. Müller, & B. L. Rozovskii (Eds.), *Stochastic Modelling in Physical Oceanography* (pp. 113–140): Birkhäuser Boston.

Haidvogel, D. B., Arango, H., Budgell, W. P., Cornuelle, B. D., Curchitser, E., Di Lorenzo, E., & Wilkin, J. (2008). Ocean forecasting in terrain-following coordinates: Formulation and skill assessment of the Regional Ocean Modeling System. *Journal of Computational Physics*, *227*(7), 3595–3624. https://doi.org/10.1016/j.jcp.2007.06.016

Hunter, J. R., Craig, P. D., & Phillips, H. E. (1993). On the use of random walk models with spatially variable diffusivity. *Journal of Computational Physics*, *106*(2), 366–376. https://doi.org/10.1016/S0021-9991(83)71114-9

Isachsen, P. E. (2015). Baroclinic instability and the mesoscale eddy field aorund the Lofoten Basin. *Journal of Geophysical Research: Oceans*, *120*, 2884–2903. https://doi.org/10.1002/2014JC010448-

Isachsen, P. E., Koszalka, I., & Lacasce, J. H. (2012). Observed and modeled surface eddy heat fluxes in the eastern Nordic Seas. *Journal of Geophysical Research*, *117*, C08020. https://doi.org/10.1029/2012JC007935

Isachsen, P. E., LaCasce, J. H., Mauritzen, C., & Häkkinen, S. (2003). Wind-driven variability of the large-scale recirculating flow in the Nordic Seas and Arctic Ocean. *Journal of Physical Oceanography*, *33*(12), 2534–2550. https://doi.org/10.1175/1520-0485(2003)033<2534:WVOTLR>2.0.CO;2

Ivanov, V., & Korablev, A. A. (1995). Formation and regeneration of the pycnocline lens in the Norwegian Sea. *Russian Meteorology and Hydrology*, *9*(9), 62–69.

Jones, C. E., Dagestad, K. F., Breivik, Ø., Holt, B., Röhrs, J., Christensen, K. H., & Skrunes, S. (2016). Measurement and modeling of oil slick transport. *Journal of Geophysical Research: Oceans*, *121*, 7759–7775. https://doi.org/10.1002/2016JC012113

Köhl, A. (2007). Generation and stability of a quasi-permanent vortex in the Lofoten Basin. *Journal of Physical Oceanography*, *37*(11), 2637–2651. https://doi.org/10.1175/2007JPO3694.1

Koszalka, I., LaCasce, J. H., Andersson, M., Orvik, K. A., & Mauritzen, C. (2011). Surface circulation in the Nordic Seas from clustered drifters. *Deep-Sea Research Part I: Oceanographic Research Papers*, *58*(4), 468–485. https://doi.org/10.1016/j.dsr.2011.01.007

Koszalka, I., LaCasce, J. H., & Mauritzen, C. (2013). In pursuit of anomalies—Analyzing the poleward transport of Atlantic Water with surface drifters. *Deep-Sea Research Part II: Topical Studies in Oceanography*, *85*, 96–108. https://doi.org/10.1016/j.dsr2.2012.07.035

Koszalka, I., LaCasce, J. H., & Orvik, K. A. (2009). Relative dispersion in the Nordic Seas. *Journal of Marine Research*, *67*(4), 411–433. https://doi.org/10.1357/002224009790741102

Kovacs, K. M., Lydersen, C., Overland, J. E., & Moore, S. E. (2011). Impacts of changing sea-ice conditions on Arctic marine mammals. *Marine Biodiversity*, *41*(1), 181–194. https://doi.org/10.1007/s12526-010-0061-0

Kvile, K. Ø., Romagnoni, G., Dagestad, K. F., Langangen, Ø., & Kristiansen, T. (2018). Sensitivity of modelled North Sea cod larvae transport to vertical behaviour, ocean model resolution and interannual variation in ocean dynamics. *ICES Journal of Marine Science*, *75*(7), 2413–2424. https://doi.org/10.1093/icesjms/fsy039

LaCasce, J. H. (2008). Statistics from Lagrangian observations. *Progress in Oceanography*, *77*(1), 1–29. https://doi.org/10.1016/j.pocean.2008.02.002

Lumpkin, R., & Pazos, M. (2007). Measuring surface currents with Surface Velocity Program drifters: The instrument, its data, and some recent results. *Lagrangian Analysis and Prediction of Coastal and Ocean Dynamics*, 39–67 (Chapter 2). https://doi.org/10.1017/CBO9780511535901.003

MacLachlan, C., Arribas, A., Peterson, K. A., Maidens, A., Fereday, D., Scaife, A. A., & Madec, G. (2015). Global Seasonal forecast system version 5 (GloSea5): A high-resolution seasonal forecast system. *Quarterly Journal of the Royal Meteorological Society*, *141*(689), 1072–1084.

Mauritzen, C. (1996). Production of dense overflow waters feeding the North Atlantic across the Greenland-Scotland Ridge. Part 1: Evidence for a revised circulation scheme. *Deep Sea Research Part 1: Oceanographic Research Papers*, *43*(6), 769–806. https://doi.org/10.1016/0967-0637(96)00037-4

Nøst, O. A., & Isachsen, P. (2003). The large-scale time-mean ocean circulation in the Nordic Seas and Arctic Ocean estimated from simplified dynamics. *Journal of Marine Research*, *61*(2), 175–210. https://doi.org/10.1357/002224003322005069

Ogawa, F., Keenlyside, N., Gao, Y., Koenigk, T., Yang, S., Suo, L., & Semenov, V. (2018). Evaluating impacts of recent Arctic Sea ice loss on the Northern Hemisphere winter climate change. *Geophysical Research Letters*, *45*(7), 3255–3263. https://doi.org/10.1002/2017GL076502

Orvik, K. A., & Niiler, P. (2002). Major pathways of Atlantic water in the northern North Atlantic and Nordic Seas toward Arctic. *Geophysical Research Letters*, *29*(19), 1896. https://doi.org/10.1029/2002GL015002

Poulain, P. M., Warn-Varnas, a., & Niiler, P. P. (1996). Near-surface circulation of the Nordic seas as measured by Lagrangian drifters. *Journal of Geophysical Research*, *101*, 18,237–18,258. https://doi.org/10.1029/96JC00506

Raj, R., Johannesen, J., Eldevik, T., Nilsen, J., & Halo, I. (2016). Quantifying mesoscale eddies in the Lofoten Basin. *Journal of Geophysical Research: Oceans*, *121*, 4503–4521. https://doi.org/10.1002/2016JC011637

Richards, C. G., & Straneo, F. (2015). Observations of water mass transformation and eddies in the Lofoten Basin of the Nordic Seas. *Journal of Physical Oceanography*, *45*(6), 1735–1756. https://doi.org/10.1175/JPO-D-14-0238.1

Rossby, T., Ozhigin, V., Ivshin, V., & Bacon, S. (2009). An isopycnal view of the Nordic Seas hydrography with focus on properties of the Lofoten Basin. *Deep-Sea Research Part I: Oceanographic Research Papers*, *56*(11), 1955–1971. https://doi.org/10.1016/j.dsr.2009.07.005

Rossby, T., Prater, M. D., & Søiland, H. (2009). Pathways of inflow and dispersion of warm waters in the Nordic Seas. *Journal of Geophysical Research*, *114*, C04011. https://doi.org/10.1029/2008JC005073

Rühs, S., Schwarzkopf, F. U., Speich, S., & Biastoch, A. (2019). Cold vs. warm water route—Sources for the upper limb of the Atlantic Meridional Overturning Circulation revisited in a high-resolution ocean model. *Ocean Science*, *15*(3), 489–512. https://doi.org/10.5194/os-15-489-2019

Segtnan, O. H., Furevik, T., & Jenkins, A. D. (2011). Heat and freshwater budgets of the Nordic seas computed from atmospheric reanalysis and ocean observations. *Journal of Geophysical Research*, *116*, C11003. https://doi.org/10.1029/2011JC006939

Shchepetkin, A. F., & McWilliams, J. C. (2005). The regional oceanic modeling system (ROMS): A split-explicit, free-surface, topography-following-coordinate oceanic model. *Ocean Modelling*, *9*(4), 347–404. https://doi.org/10.1016/j.ocemod.2004.08.002

Shchepetkin, A. F., & McWilliams, J. C. (2009). Correction and commentary for "Ocean forecasting in terrain-following coordinates: Formulation and skill assessment of the regional ocean modeling system" by Haidvogel et al., J. Comp. Phys. 227, pp. 3595-3624. *Journal of Computational Physics*, *228*(24), 8985–9000. https://doi.org/10.1016/j.jcp.2009.09.002

Spall, M. A. (2010). Dynamics of downwelling in an eddy-resolving convective basin. *Journal of Physical Oceanography*, *40*(10), 2341–2347. https://doi.org/10.1175/2010JPO4465.1

Trodahl, M., & Isachsen, P. E. (2018). Topographic influence on baroclinic instability and the mesoscale eddy field in the northern North Atlantic Ocean and the Nordic Seas. *Journal of Physical Oceanography*, *48*(11), 2593–2607. https://doi.org/10.1175/JPO-D-17-0220.1

Umlauf, L., & Burchard, H. (2003). A generic length-scale equation for geophysical turbulence models. *Journal of Marine Research*, *61*(2), 235–265.

van Sebille, E., Griffies, S. M., Abernathey, R., Adams, T. P., Berloff, P., Biastoch, A., & Zika, J. D. (2018). Lagrangian ocean analysis: Fundamentals and practices. *Ocean Modelling*, *121*(October 2017), 49–71. https://doi.org/10.1016/j.ocemod.2017.11.008

Volkov, D. L., Belonenko, T. V., & Foux, V. R. (2013). Puzzling over the dynamics of the Lofoten Basin—A sub-Arctic hot spot of ocean variability. *Geophysical Research Letters*, *40*, 738–743. https://doi.org/10.1002/grl.50126

Volkov, D. L., Kubryakov, A. A., & Lumpkin, R. (2015). Formation and variability of the Lofoten basin vortex in a high-resolution ocean model. *Deep-Sea Research Part I: Oceanographic Research Papers*, *105*, 142–157. https://doi.org/10.1016/j.dsr.2015.09.001

Wagner, P., Rühs, S., Schwarzkopf, F. U., Koszalka, I., & Biastoch, A. (2019). Can Lagrangian tracking simulate tracer spreading in a high-resolution Ocean General Circulation Model? *Journal of Physical Oceanography*, *49*(5), 1141–1157. https://doi.org/10.1175/JPO-D-18-0152.1

Warner, J. C., Sherwood, C. R., Arango, H. G., & Signell, R. P. (2005). Performance of four turbulence closure models implemented using a generic length scale method. *Ocean Modelling*, *8*(1-2), 81–113.